Supplementary figures

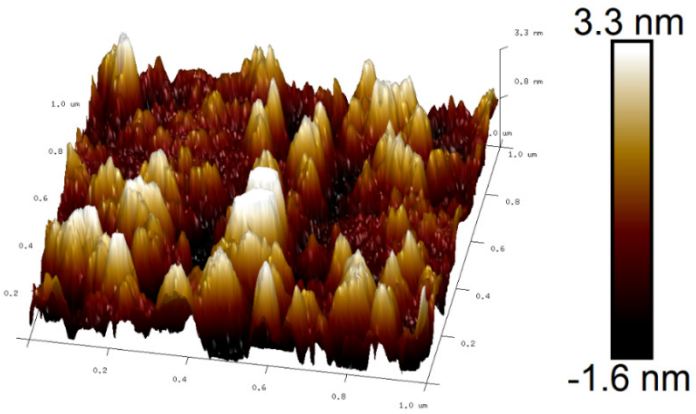

Figure S1. AFM image of the $MgCO_3$ nanosheet and height profiles along the dashed lines in AFM image.

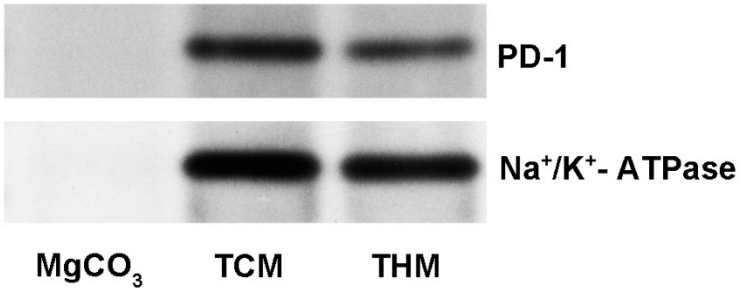

Figure S2. Western blot analysis of Na^+/K^+- ATPase and PD-1 proteins in different formulations.

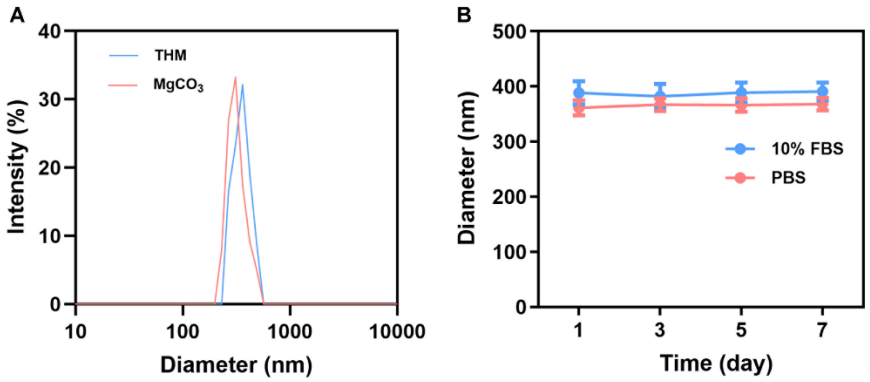

Figure S3. (A) The particle size distribution of different nanomaterials. (B) Stability of

THM in various solutions at different times. Data are shown as the mean ± SD (n = 3).

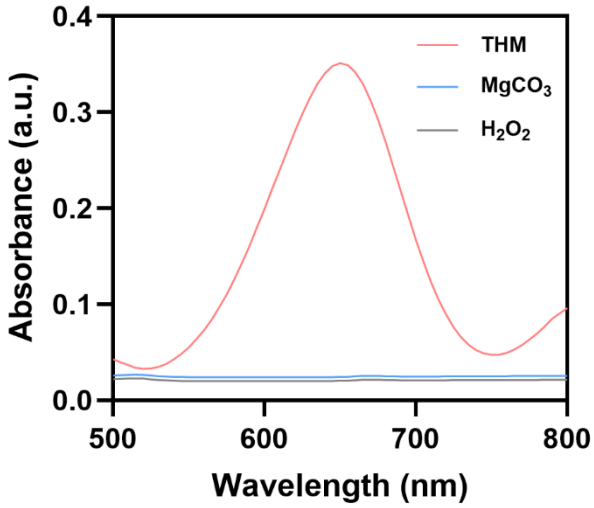

Figure S4. Oxidation of TMB due to generated •OH by indicated treatments.

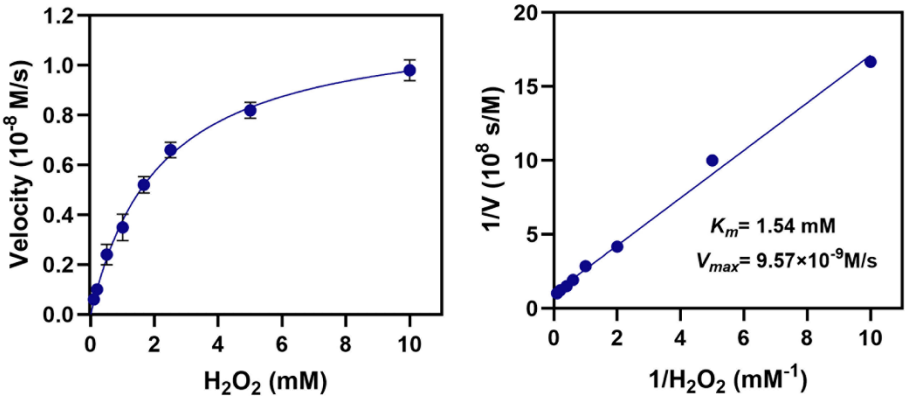

Figure S5. Initial velocity of the reaction with varied concentration of H_2O_2 and the double-reciprocal plots of H_2O_2. Data are shown as the mean ± SD (n = 3)**.**

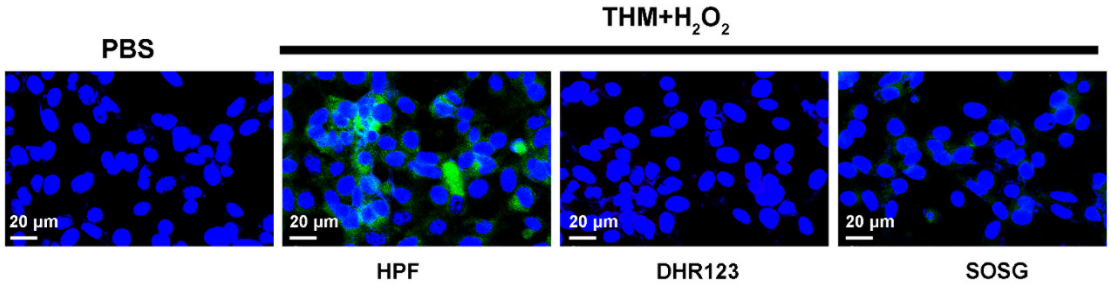

Figure S6. CLSM images of different types of ROS generated in 4T1 cells upon

different treatments. Blue: DAPI.

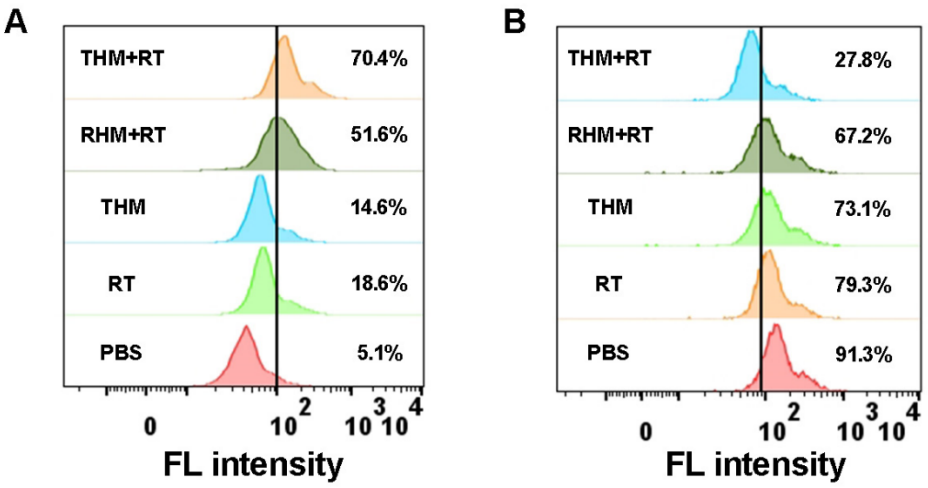

Figure S7. (A) Fluorescence-activated cell sorting (FACS) micrograph of CRT and (B) HMGB1 expression in nanoparticles-treated 4T1 cells.

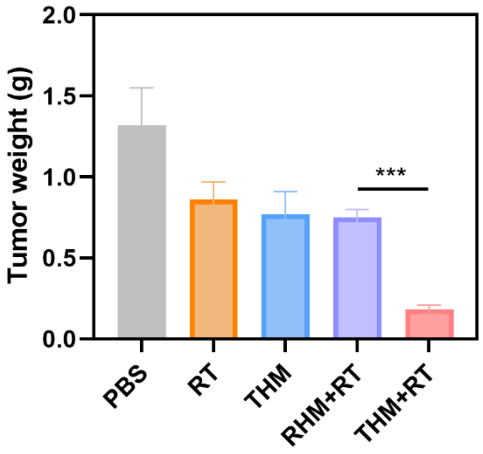

Figure S8. Tumor weight after different treatments. Data are shown as the mean ± SD (n = 5).

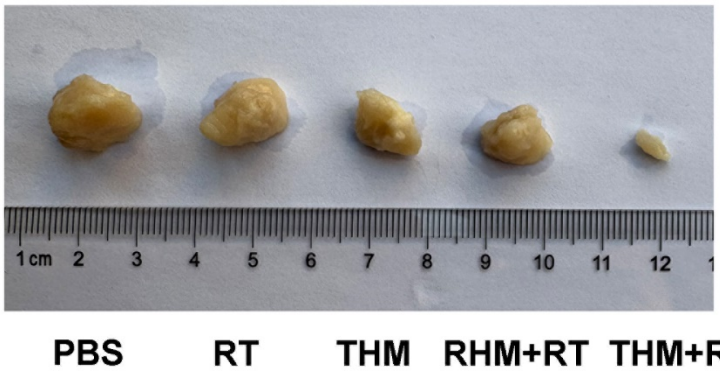

Figure S9. Representative tumor pictures after different treatments.

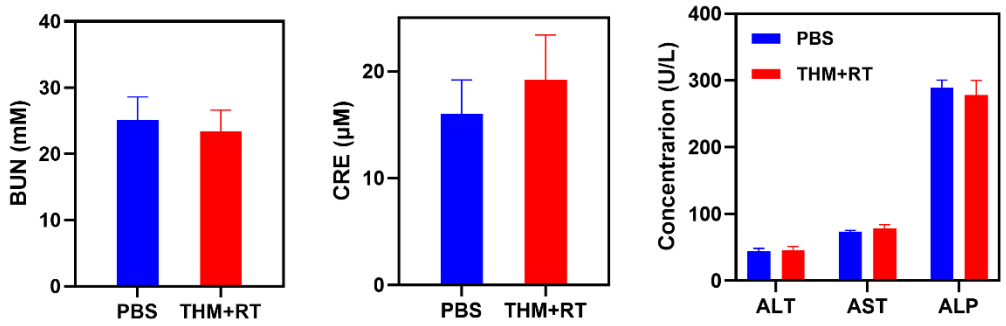

Figure S10. Analysis of liver and kidney function indicators. Data are shown as the mean ± SD (n = 5).

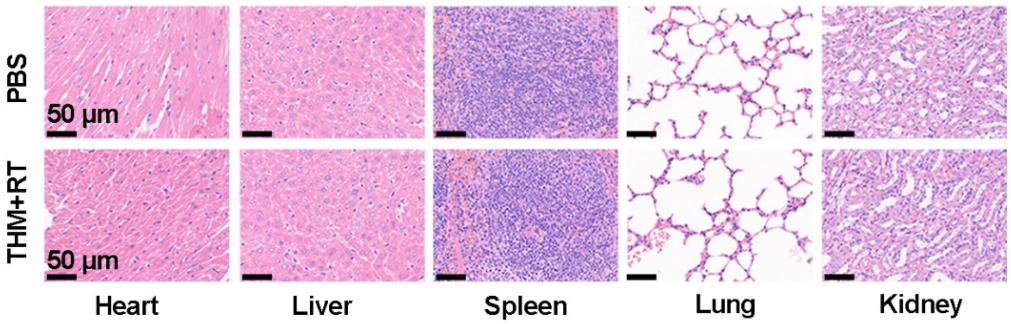

Figure S11. HE sections of major organs after different treatments.

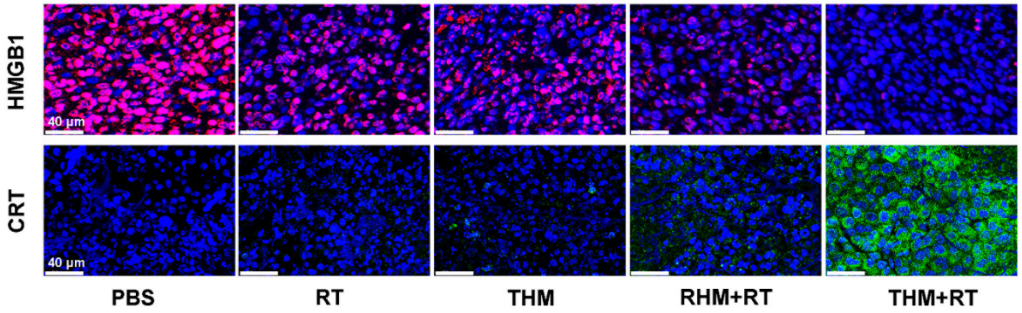

Figure S12. CRT and HMGB1 staining of tumor sections after the indicated treatments.